JAAS

ROYAL SOCIETY OF CHEMISTRY

PAPER

View Article Online
View Journal | View Issue

Cite this: *J. Anal. At. Spectrom.*, 2023, **38**, 2636

An optimized chromatography method and MC-ICP-MS technique for apatite Lu–Hf geochronology

Chao Zhang, * Tsai-Wei Chen and Jeffrey D. Vervoort

Apatite is a common accessory mineral found in almost all igneous, metamorphic, and clastic sedimentary rocks. It contains concentrations of lutetium and hafnium amenable to dating by the Lu–Hf isochron method. However, the application of this method has been hampered by chemical difficulties associated with the extraction of a clean Hf concentrate from apatite. A novel method of efficient chemical separation utilizing Ln and DGA-normal extraction chromatography columns has been developed for precise isotope analysis and is presented in this study. The routine analysis of sub-ng amounts of Hf maintained high yield close to 100%. The purification of Hf with a DGA-normal chromatography column effectively eliminated the interfering elements (Yb, Lu, and W), typically resulting in less than 1 pg of Lu in the analyzed apatite Hf solution. Apatite Lu–Hf isotope compositions of Otter Lake, Bancroft, and Durango apatites were determined using the reported methodology and yielded isochron ages of 1047.6 ± 3.4 Ma, 1092 ± 17 Ma, and 31.1 ± 1.1 Ma, respectively. All apatite Lu–Hf isochrons are characterized by phenomenally high apatite $^{176}Lu/^{177}Hf$ and $^{176}Hf/^{177}Hf$ ratios. Such apatite Lu–Hf isochrons are shown to be not significantly dependent on the initial isotopic composition in determining accurate and precise ages, allowing for anchoring the low end of the isochron with an estimated isotopic composition.

Received 20th June 2023
Accepted 11th October 2023

DOI: 10.1039/d3ja00203a

rsc.li/jaas

Introduction

Apatite, broadly, refers to three calcium phosphate minerals – fluorapatite, chlorapatite, and hydroxyapatite – represented by the general formula $Ca_5(PO_4)_3(Cl, F, OH)$. It is the most abundant phosphorus mineral on Earth and plays an essential role in forming the teeth and endoskeleton for a variety of species. This mineral is also geologically ubiquitous, commonly occurs as an accessory mineral in igneous, metamorphic, and sedimentary rocks, and has been found in meteorites and in samples returned from the Moon (*e.g.*, Jones *et al.*,[1] Boyce *et al.*[2]). Its ubiquity has resulted in many applications in fields of study ranging from agronomy, biology, medicine, dentistry, and materials science (*e.g.*, Rakovan and Pasteris[3]). The geological significance of apatite further arises from its highly variable chemical composition which is a result of its crystal structure being able to accommodate many elements.[4] As its chemical formula indicates, the anions are dominated by F, Cl, OH, or a solid solution among these endmembers. Apatite is the major reservoir for these halogens, as well as P and REE in most rocks, and CO_2 in some rocks. The partitioning of these elements between apatite and co-existing minerals, melt, and fluid has yielded applications to magmatic, magmatic-hydrothermal, and metasomatic processes, such as tracking the fluid interaction in igneous and metamorphic rocks (*e.g.*, Doherty *et al.*,[5] Hansen and Harlov,[6] Sallet[7]) and modelling the behaviors of volatile and non-volatile elements during magma genesis and evolution and during magmatic-hydrothermal ore formation (*e.g.*, Harlov *et al.*,[8] Krause *et al.*,[9] Palma *et al.*[10]).

The cation site, dominated by Ca, can also host many substituents, including Sr, REE, Th, and U. Based on these varying chemical compositions, four radiogenic isotopic geochronometers have been developed: fission track, (U–Th)/He, U–Pb, and Lu–Hf – each with a different temperature for isotopic closure.[11] The fission track and (U–Th)/He methods have been widely applied in studying low temperature upper-crustal and near-surface processes (*e.g.*, Chew and Donelick[12]), whereas the U–Pb and Lu–Hf systems, with higher closure temperatures (apatite Lu–Hf: above 650 °C),[11] have the potential for dating the thermal, tectonic, and magmatic events in the deeper crust (*e.g.*, Barfod *et al.*,[13] Kirkland *et al.*,[14] Larsson and Söderlund,[15] Thomson *et al.*[16]).

The REE concentration of apatite ranges from tens to several thousand ppm (μg g^{-1}). Hosting ample Lu, apatite is an excellent candidate for Lu–Hf isochron age dating. However, it has one important caveat in its critically low Hf content, typically between a few and a few tenths of ppb (ng g^{-1}), which may explain its limited use as a Lu–Hf chronometer at present. Despite this challenge the great potential in apatite should be recognized. As demonstrated by several successful Lu–Hf geochronology studies, apatite was in fact successfully

School of the Environment, Washington State University, Pullman, WA, 99164, USA

employed in determining the ^{176}Lu decay constant[17–19] and it is applicable in dating magmatic and metamorphic events[13,15,19] and even animal teeth,[13] while also addressing the significant role of phosphates in disturbing chondrite Lu–Hf geochronology.[20] The highly contrasting Lu, Hf concentrations result in isochrons with significant spread of parent–daughter ratios, which generate precise ages. Furthermore, this method may also provide the possibility of dating some difficult to date, such as mafic to ultramafic rocks that generally lack datable minerals like zircon and baddeleyite.[15]

Ultimately, in order to cope with the low Hf content in apatite, effective chemical separation is essential, and precise mass spectrometry analysis is key. Both are necessary for developing apatite Lu–Hf geochronology to its full potential and achieving a broader application. In this study, we will address these challenges, discuss several aspects of apatite chemistry to provide information on solution-based age dating and Lu–Hf column chromatography with the ultimate goal of proposing an optimized procedure for apatite Lu–Hf geochronology.

Background

Mineral dissolution

Many solution-based analyses in geology require complete dissolution of the rock or mineral. When redox reactions are not often considered, the dissolution of a mineral in acidic solution consists of two interdependent reactions. One reaction involves the interaction of H^+ or H_3O^+ on the mineral surface, leading to the release of anions, while the other reaction occurs between the metal cation in the mineral and a complexing agent in the solution (*e.g.*, Cl- and water). When dissolving by non-complexing acids (*e.g.*, nitric, sulfuric, and perchloric acids), no strong complexing anions are present and the predominant species of many metals are their complexes with water molecules (*i.e.*, metal aquo complexes).[21] The digestion of silicate minerals or rocks is normally achieved by either HF–HNO_3 acid dissolution[22] or flux melting supported dissolution.[23,24] The HF–HNO_3 dissolution takes advantage of the ability of hydrofluoric acid to decompose silicates and form the volatile compound SiF_4 which can be fumed out of the sample.

$$SiO_x^{4-2x}(s) + 4\ HF(aq) + (2x - 4)\ H^+(aq) = SiF_4(g) + xH_2O$$

The excess fluorine is subsequently removed either by reacting with orthoboric acid[25] or by fuming with perchloric acid.[22,26] The boric acid removes fluorine by preferentially bonding with F^- to form the evaporative BF_3. Removing hydrofluoric acid by fuming with perchloric acid utilizes their different boiling temperatures. The boiling temperatures of both HF and HCl acids are low, about 110–120 °C, while the boiling temperature of perchloric acid is 160 °C. Therefore, when the solution is gradually warmed up, HF acid will evaporate first and escape from the solution. This method is quite versatile, as the strong acid mixture is effective in dissolving major silicate/oxide rocks and minerals, making it by far the most common dissolution method for Hf isotope geochemistry.[27–31] The removal of silicates and fluorine allows the metals in the solution to be converted to chlorides, nitrates, or aquo complexes, which are the preferred forms in subsequent elemental chromatography extractions.

Chemical separation

Many chemical separation techniques have been used to assay certain elements in various earth materials, including solvent extraction, selective precipitation, ion exchange chromatography (IEC), and extraction chromatography (EXC). The latter two have become increasingly popular in modern geochronology studies, where elemental separation is usually accomplished by using one or multiple columns.[21,25,32–34] The function of IEC resin is based on electrostatic interaction between the oppositely charged stationary column and ions in the mobile phase. IEC resins do not provide enough separation for some ions with similar charge and radius (*e.g.*, Lu and Yb) and are often used as an initial capture. Commonly used IEC resins include the strong acid cation exchange resin (*e.g.*, Bio-Rad AG® 50W) and strongly basic anion exchange resin (*e.g.*, Bio-Rad AG®1). EXC resins exploit complex-forming or chelate-forming extractants absorbed onto an inert polymeric support (*e.g.*, Eichrom TRU, Ln, Pb, Sr, DGA resins). EXC resins are highly specific for a particular element or a group of elements and are therefore often used as an intermediate purification step or a final polishing step.

Regardless of the type of chromatography column being used, an effective separation requires the sample to be introduced to the resin in a proper solution. It is crucial that the elements of interest are converted into the proper species in this solution. For example, a garnet dissolution is introduced to the cation exchange column in a 1 M HCl/0.05 M HF solution in which Hf is complexed with F forming $[Hf{\cdot}F_{4-6}]^{0\sim-2}$ whereas other metal cations are probably present as aquo complexes (*e.g.*, $[Ca(H_2O)_6]^{2+}$). The neutral to negatively charged Hf complex will not be absorbed while other cations being readily retained by the resin. The preliminary separation of Hf is thus achieved.

Apatite chemistry

Several aspects of apatite chemistry pose potential challenges to the extraction of a clean Hf concentrate. Resolving these problems is essential for the successful development of the apatite Lu–Hf method.

Apatite has critically low Hf contents. The natural Hf concentration in apatite is generally below 10 ppb. To obtain enough hafnium for accurate analysis, one may have to separate a considerable amount of apatite, which is often not practical for some samples. Therefore, it is crucial to keep Hf loss to minimum and to recover as close to 100% of Hf from the sample as possible during the chemical separation process.

Apatite dissolves easily but results in a complicated solution. Compared to silicate minerals, apatite dissolves readily in most laboratory acids such as HCl and HNO_3. The dissolution of apatite is essentially a matter of acidity and produces soluble

hydrogen phosphate and dihydrogen phosphate ions. Both have the ability to buffer the acidity of the solution.

$$Ca_5(PO_4)_3(Cl, F)(s) + 3H^+ = 5Ca^{2+} + 3HPO_4^{2-}(aq) + Cl^-, F^-$$

$$Ca_5(PO_4)_3(Cl, F)(s) + 6H^+ = 5Ca^{2+} + 3H_2PO_4^-(aq) + Cl^-, F^-$$

The resultant solution is much more complicated than that of a silicate mineral due to the presence of several anions including PO_4^{3-}, HPO_4^{2-}, $H_2PO_4^-$, and F^-, all of which are strongly complexing.[35,36] The buffering effect and the complexation reaction between Hf and several competing anions are concerning in the chromatographic separation of an apatite solution.

Insoluble calcium salts prevent the use of HF or H_2SO_4 acids. Calcium is a major component of apatite and is insoluble when bonded with F^- or SO_4^{2-}. There is no benefit in employing HF acid in the dissolution of apatite as it does not break down phosphate as it does with silicates. HF acid is often used to produce the Hf complex when needed and is used to stabilize Hf from hydrolysis. However, such steps would need to be taken with caution as applying even trace amount of HF acid to apatite solution forms CaF_2 precipitate which not only does not go into the solution but also causes co-precipitation of other elements including Hf.

Last, but not least, the common fluorapatite form requires different chemical treatment due to its high fluorine content. Up to ~3.7 wt% of fluorine could be incorporated in apatite's crystal structure, which means that the apatite dissolution forms a significant amount of hydrofluoric acid. The F^- in the resultant solution is also complexing, even more strongly than PO_4^{3-}. The resultant Hf–F complex would affect the uptake of Hf onto virtually all types of exchange resin. Such apatite would need to be treated either with orthoboric acid or fumed with perchloric acid. However, the effectiveness of both has been undermined by the presence of phosphate ion.[37]

In conclusion, the complexity of apatite solutions is due to the presence of at least three types of anions in the solution that complete to from complexes with Hf, which poses a challenge for Hf separation. In this study, we explore the applicability of specialized extraction chromatographic resins and propose an optimized method for apatite Lu–Hf separation. As a demonstration, we also present three apatite Lu–Hf ages determined following this methodology.

Methodology

Mineral separation. Depending on the hafnium concentration of the apatite, the amount of apatite to be separated varies from 0.1 to 1 g. For Hf analysis in our lab, we consider 1 ng Hf to be the minimum amount for an accurate analysis and therefore the weight of apatite is calculated based on the Hf concentration to ensure at least that amount of hafnium is dissolved into the solution. The separation procedure differs for different types of rocks but generally requires hand magnet screening, Franz magnetic separation, and density separation. Apatite gradually becomes susceptible when the magnetic field is at ~1.2 amp. Apatite has a specific gravity of 3.16–3.22 g per cc and is separated from the light mineral fraction in an acetone-diluted methylene iodide (MEI) heavy liquid solution, whose specific gravity is ensured to be 3 g per cc. The removal of zircon is done in regular MEI with a specific gravity of 3.3 g per cc, where apatite floats.

Dissolution. The apatite dissolution is done using HCl acids. The apatite concentrate is first lightly rinsed with ~1 M HCl for no longer than 15 seconds to remove any surficial contamination from the physical separation. Carbonate inclusions are decomposed simultaneously during the rinsing process. The HCl rinse is carefully pipetted out without disturbing the settled apatite fractions and discarded. The apatite separates are then rinsed twice in deionized water. The digestion of the rinsed apatite takes place in ~4 ml 6 M HCl in a 15 ml Savillex beaker heated at 100 °C for 24 hours. Typically, the solution appears clear to unaided eyes in two hours, indicating the dissolution of apatite. The sample solution is then centrifuged at 3500 rpm for 15 minutes, to remove the insoluble material, and is then ready for spiking.

It is not recommended to substitute HCl with HNO_3 acid, although the same dissolution can be achieved. HCl acid is an evaporative and complexing acid. Most of the metal cations dry as chloride salts in HCl acid and re-dissolve easily. HNO_3 acid is evaporative but not complexing; most metals, including Hf, thus precipitate as hydrated oxides when dried in HNO_3 and are sometimes difficult to re-dissolve, especially the Hf oxide precipitate (product of hydrolyzed Hf).

Attempts were made to remove the natural fluorine from fluorapatite solution. For the two fluorapatite samples that underwent perchloric acid fuming, no significant increase in Hf uptake was observed in the first stage chemical separation. This indicates that the removal of fluorine is not always successful. One possible explanation is that some fluoride complexes, Hf–F specifically, are very stable. Once they form the coordination compounds, it is difficult for the fluoride ion to go back to the solution and evaporate as fluoric acid.[37] It is also possible that the fuming is affected by the abundant phosphate causing the solution to saturate. We have noticed the fuming solution dries out before the complete evaporation of the perchloric acid. Therefore, the perchloric acid fuming step was not adopted in our method.

Spiking. Next, the solution is spiked with a ^{176}Lu–^{180}Hf mixed isotope tracer. The spiking is usually aimed at obtaining a mixed $^{180}Hf/^{177}Hf$ ratio of 2.3 to keep error magnification in spike calibration at a minimum. However, because apatite is poor in Hf, the Hf is sometimes over-spiked while Lu is inevitably under-spiked, even for a high Lu/Hf spike designed for garnets. The sample solution is then capped and equilibrates on a hotplate for 24 hours and then dries down. The sample should dry down after spiking to ensure that any conversion of Lu and Hf to different species during the drying process occurs in both the sample and spike in the same proportion. The dried sample is then re-dissolved with 1–2 ml of 3 M HCl acid and ready for chromatography.

Chromatography. The elemental separations are carried out using two-stage chromatographic columns (Fig. 1, Table 1). The

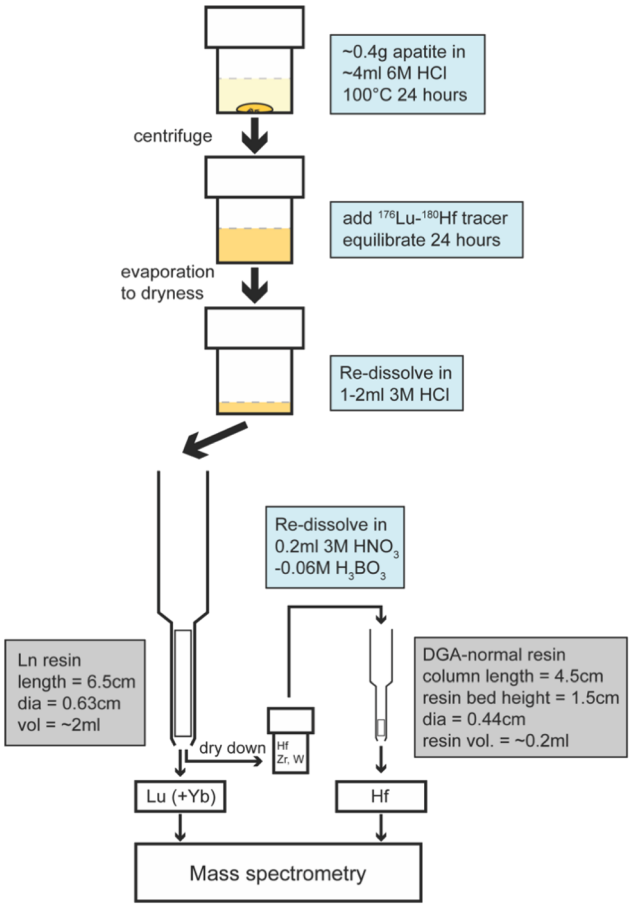

Fig. 1 Cartoon showing workflow of Lu–Hf apatite method.

first stage employs a 2 ml resin bed volume of Eichrom Ln resin (part no. LN-B50-A) with a particle size of 100–150 μm to concentrate Hf and reduce the Yb/Lu ratio in the Lu cut. The Lu extract after this stage is ready for mass spectrometry analysis, whereas the Hf fraction needs to be further purified on the second-stage column. The second-stage column is modified after Connelly *et al.*[38] and uses a 0.2 ml resin bed volume of Eichrom DGA-normal resin (part no. DN-B25-S) with a particle size of 50–100 μm. The DGA-normal resin is coated with chelate forming extractant that preferentially bonds trivalent metal ions and is intended to separate the REEs from hafnium. The recovery of hafnium on the DGA-normal column is close to 100%. Because both columns utilize resins that specialize in separating trivalent REEs while retaining little matrix elements, the column sizes are much smaller than conventional fast-flowing cation exchange resin columns. Smaller columns and shorter chemical processes have the advantages in returning higher Hf yield and using less amount of wash acids which are a benefit for lower blanks. This two-stage chemistry process is well suited for the apatite element separation and hafnium purification. After the two-stage separation, the amount of Lu in the Hf concentrate is typically reduced to less than 1 pg (see section of "Uncertainty assessment" below).

1st stage separation on Ln column. The complete separation scheme and elution curves are presented in Table 1 and Fig. 2, respectively. Based on the working capacity of the 100–150 μm Ln resin (0.012 mmol ml^{-1} or 1.8 mg of Eu per ml), the volume of resin is determined to be 2 ml to accommodate the abundant REE in apatite. The Eichrom Ln resin consists of an HDEHP (di(2-ethylhexyl) orthophosphoric acid) coating on an inert polymeric carrier. This resin specializes in separating REEs and has been employed in many studies.[34,39,40] The Hf retention is

Table 1 Elution schemes for the two-stage apatite Lu–Hf chromatographic separation

Step	Acid and volume[a]
Column I: Ln resin (2 ml)	
Clean	10 rv ~2 M HF
	10 rv ~6 M HCl
Pre-condition	5 ml 3 M HCl
Load sample	2 ml 3 M HCl
Elute matrix, LREE, some Yb	35 ml 3 M HCl
Collect Lu, remaining Yb	12 ml 6 M HCl
Rinse	4 ml H_2O
Elute Ti	15 ml 0.45 M HNO_3 – 0.09 M Hcit – 1 wt% H_2O_2
Wash off H_2O_2	5 ml 0.45 M HNO_3
Collect Hf	12 ml 8 M HNO_3 – 0.4 M HF
Column II: DGA-normal resin (0.2 ml)	
Clean	10 rv 1 M HNO_3 – 0.2 M HF
	30 rv 0.05 M HCl
Pre-condition	10 rv 3 M HNO_3 – 0.06 M H_3BO_3
Load	0.2 ml 3 M HNO_3 – 0.06 M H_3BO_3
Rinse	0.2 ml 3 M HNO_3 – 0.06 M H_3BO_3
Elute Ti, Fe	4.5 ml 3 M HNO_3
Elute Zr	10 ml 0.1 M HNO_3
Collect Hf	10 ml 3 M HNO_3 – 0.2 M HF

[a] rv: resin volume (2 ml for Ln column, 0.2 ml for DGA-normal column).

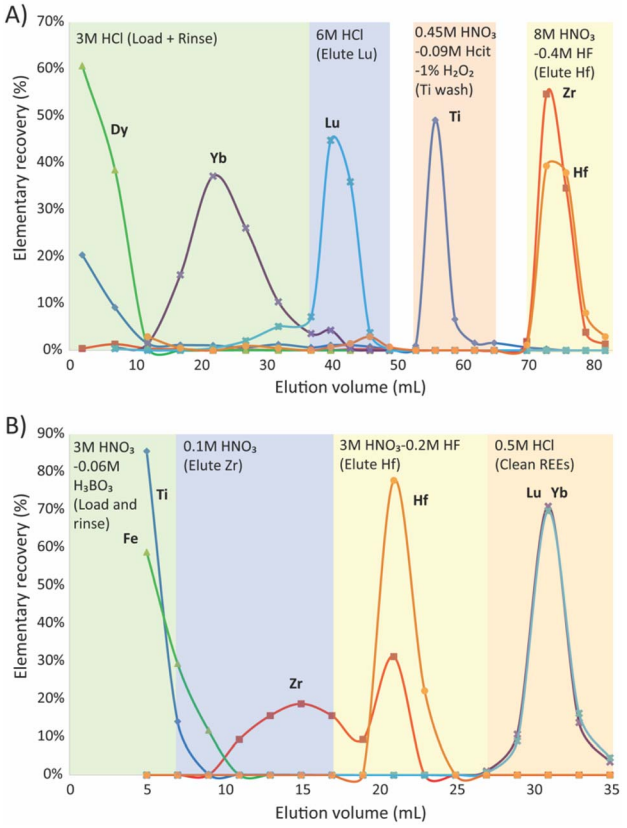

Fig. 2 Elution schemes for a natural apatite solution (Otter Lake apatite) on Ln column (A) and subsequent Hf purification on DGA-normal column. (B) Elutes were normalized to the total amounts loaded.

extremely high from 0.1 to 8 M HNO_3 or HCl acids when strong complexing agents, for instance, F^-, PO_4^{3-}, and HEDPA (hydroxyethanediphosphonic acid), are not present (Eichrom, personal commun.). For an apatite solution, the uptake of Hf will certainly be affected by F^- and PO_4^{3-}. However, based on several experiments, it was found that the Ln resin showed extraction of Hf even in apatite solutions where it is not completely free from complexing anions. The possible reason for this is that the complexing ability of the extractant of HDEHP is comparable to that of the phosphoric acid as both the ligands are phosphoryl oxygen. The overall uptake of Hf can be improved by loading sample in the smallest volume in which it can completely dissolve, typically less than 2 ml. In this way, the sample solution encounters clean, Hf-free resin as it flows down the column which ensures the continuous partitioning of Hf onto the resin. The acidity of the loading solution is 3 M based on the retention of other interfering cations. Major elements including the alkali metals, the alkaline earth metals, and lead have low distribution coefficients in strong (>0.1 M) HCl or HNO_3 acids.[41] Fe(III) shows minimum retention in HCl acid at 3 M. Light REEs are not retained by the resin when the acidity is higher than 1 M.[34] Therefore, 3 M HCl or HNO_3 acids are appropriate solutions with which to introduce apatite to the resin.

Upon loading, the columns are washed with 35 ml of 3 M HCl acid. The matrix and the LREE are eluted at the beginning of the wash followed by Fe(III). The 3 M HCl acid wash has eliminated the use of ascorbic acid (*e.g.*, used in the Münker *et al.*[34] chemistry) which reduces Fe(III) to Fe(II) for a quicker iron washout. Yb and Lu come out as two separate peaks. The volume of the wash is calibrated to ensure the elimination of the majority of Yb but little Lu. The remaining Lu on the column is usually 2–10 times the amount of remaining Yb. Both Lu and Yb are then collected in 12 ml 6 M HCl acid. Some Yb must remain in the Lu cut to allow for the correction of mass fractionation and machine bias during mass spectrometry.[42] The Lu concentrate is dried down and ready for mass spectrometry analysis. Titanium is rinsed off the column using 15 ml of 0.45 M HNO_3 – 0.09 M citric acid – 1 wt% H_2O_2 mixed acid. To avoid partial loss of the HFSE in the HCl–H_2O_2 mixtures, the columns are rinsed with 4 ml H_2O before the Ti elution. This mixed acid wash is an effective chelating agent for titanium, and the formed titanium complex has an orange color. Because the titanium content in apatite is typically low, the characteristic orange color of Ti–H_2O_2 complex is not apparent. Peroxide was then washed from the column using 5 ml of 0.45 M HNO_3 prior to the collection of hafnium. The hafnium is then eluted using 12 ml of 8 M HNO_3 – 0.4 M HF mixed acid. We tested eluting Hf with acid mixtures of different acidity in attempt to prevent the tailing of Lu and Yb into the Hf peak. This tailing, however, could not be completely eliminated which made further purification of Hf necessary. Eluting with HNO_3 acid instead of HCl is required because low molarity of chlorine will cause REE breakthrough on the next stage column. The hafnium solution to be loaded on to the second stage column needs to be essentially chlorine free.

2nd stage separation on DGA-normal column. The complete elution scheme and the elution curves are shown in Table 1 and Fig. 2. The DGA-normal resin is a synthesized tridentate ligand extraction resin developed by Eichrom Technologies Inc. and is designed to effectively separate trivalent actinides. In spite of some interest in this versatile resin,[38,43] the full potential of DGA-normal and its prospective applications to the broad field of analytical geochemistry remain largely unexplored. The extractant complexes trivalent metal ions through the formation of chelate rings which differ from the monodentate extractant of the Ln resin, resulting in strong absorption of the REE.

To prepare the columns, the dry resin is pre-cleaned in bulk in a Savillex beaker with multiple rinses of 0.05 M HCl and the resin is packed into the exchange columns after the resin is thoroughly wet. The column is cleaned with 10 resin volumes (1 rv = 0.2 ml) of 1 M HNO_3 – 0.2 M HF mixed acid and then 30 resin volumes of 0.05 M HCl acid intended to remove HFSE and REE, respectively. The column is pre-conditioned before sample loading with 3 M HNO_3 – 0.06 M H_3BO_3 mixed acid.

The Hf–Zr fraction from Ln column is first dried down and then re-dissolved in 0.2 ml 3 M HNO_3 – 0.06 M H_3BO_3 mixed acid to convert the dissolved fluoride from the previous Ln column to BF_3 gas. The dissolved sample is then loaded onto the pre-conditioned DGA-normal column. As the column is also

pre-conditioned with the same nitric boric acid, the solution Hf ions will be retained along with REE. This is followed by additional 0.2 ml 3 M HNO_3 – 0.06 M H_3BO_3 acid rinse to ensure proper sample loading. Hf, Zr, and W are retained by DGA-normal resin while any remaining Ti and Fe are washed off with 4.5 ml 3 M HNO_3. Zr has fairly low distribution coefficient with the DGA-normal resin, although greater than 1.[43,44] Therefore, it is slowly washed out with 10 ml of 0.1 M HNO_3 without breakthrough of Hf. Hf is subsequently eluted with 10 ml of 3 M HNO_3 – 0.2 M HF mixed acid. At this point, only W and REEs are retained on the column. They are retained in HNO_3 acid and are released from the resin in HCl acid. For example, the distribution coefficient for Lu is greater than 1000 in >0.05 M HNO_3 acid and is at its minimum (<5) in 0.5 M HCl acid.[43] Because the minimum distribution coefficients are still above 1, it requires at least 20 ml of 0.5 M HCl acid to wash them off thoroughly.

The chromatographic method presented in this paper represents a significant departure from the traditional cation exchange resin separation method. Unlike the latter, which hinges on forming Hf–F complexes, our method offers an alternative approach that is particularly applicable when dealing with phosphate mineral solutions. As elaborated in section of "Apatite chemistry", the inherent complexity of apatite solution matrices, compounded by the formation of calcium fluoride, introduces unpredictability when attempting to create Hf–F complexes within an apatite solution. In contrast, our current approach circumvents this dependency on Hf–F formation and utilizes the Ln extraction resin, which exhibits a complexing ability either comparable to or stronger than various phosphate ions. This enables the efficient extraction of Hf from the intricate matrix. Furthermore, within the same column, we have successfully prepared the Lu fraction.

It is not uncommon to extract Hf from an Ln column without additional purification. However, because Hf is collected after Lu on the Ln column, there will always be some residual Lu tailing into the Hf fraction. The difference between purifying Hf using DGA-normal and cation exchange resin lies in their respective mechanisms. The DGA-normal resin facilitates Hf uptake onto the column thus allowing for the relatively liberal use of boric acid in the preparation step where fluorine is consumed and Hf is restored to its aqueous form. Purification using cation exchange resin, on the other hand, still relies on the formation of Hf–F complexes. This poses a challenge when Hf levels in the solution are low, as the introduction of additional fluorine also leads to the complexation of REEs. This unintended consequence defeats the primary objective of purifying Hf from residual Lu.

In summary, our novel chromatographic method offers a more reliable and efficient means of Hf extraction from complex matrices, particularly phosphate mineral solutions, when compared to traditional cation exchange resin separation methods. Additionally, it provides insight into the nuanced differences between purifying Hf using DGA-normal and cation exchange resin, highlighting the advantages of our approach in addressing the challenges associated with low Hf concentrations.

Isotope analyses. The isotopic analyses for hafnium (Hf) and lutetium (Lu) were conducted at Washington State University Radiogenic Isotope and Geochronology Laboratory. Throughout the method's development, significant laboratory upgrades were implemented, leading to the acquisition of data initially on the Neptune MC-ICP-MS and subsequently on the Neptune Plus MC-ICP-MS. In this description, the focus will be on the more advanced and refined method, specifically developed for the instrumentation build around the Neptune Plus mass spectrometer. The Neptune Plus MS is fitted with the X skimmer cone and Jet sample cone. Paired with the Apex Ω desolvating nebulizer system operating at an uptake rate of approximately 100 μl min^{-1}, it yielded a ~0.3 V signal for ^{177}Hf from a 2 ppb JMC 475 Hf solution. In comparison, the Neptune MS, utilizing a standard sample cone and the Cetac Aridus nebulizer at an uptake rate of around 70 μl min^{-1}, yielded a signal of ~0.6 V for ^{177}Hf from a 10 ppb JMC 475 Hf solution. During the Hf sample measurements, calibration was performed relative to an external Hf standard of either 2 ppb or 10 ppb, depending on the type of MS utilized. The main isotopes of Hf (^{176}Hf, ^{177}Hf, ^{178}Hf, ^{179}Hf, and ^{180}Hf) and one of each interfering element (^{173}Yb, ^{175}Lu, and ^{182}W) are measured simultaneously. Each analysis consists of a block of 80–120 integrations of 4.2 seconds. Within this block, about 30 integrations are allocated for measuring the background of the solution. By measuring the background and the sample in a single block, we can promptly extract the available ratio measurements as soon as the sample signal arises, thereby eliminating the dead-time associated with transitioning from the background to the sample block. This approach allows for a marginally more efficient consumption of the sample solution. In instances where the Hf concentration of the sample is notably low, we adapt the integration time to a reduced duration of 2 seconds. Exponential mass bias correction and Boelrijk spike correction are applied using $^{179}Hf/^{177}Hf = 0.7325$ and $^{180}Hf/^{177}Hf = 1.88666$ for the Hf isotope ratios. Sample analyses are interspersed with analyses of the JMC 475 Hf solution and all values are normalized to a $^{176}Hf/^{177}Hf$ of 0.282160 for that standard.[45] Procedures for Lu analysis follow that described in Vervoort *et al.*[42]

Uncertainty assessment. The scatter of an isochron is evaluated by statistical MSWD which compares the scatter expected given the reported analytical uncertainty to the actual scatter of data from an isochron. If MSWD equals to 1, the observed scatter can be explained by the analytical uncertainty alone. When the analytical uncertainties of each isochron points are correctly assigned, MSWD greater than 1 indicates true geologic scatter which means that at least one of the fundamental isochron assumptions has been violated. On the other hand, underestimating the analytical uncertainty, which is often the case for apatite, will yield significantly higher MSWD values that do not necessarily reflect the true geological scatter. The scatter is also accounted for in age calculations; if analytical uncertainty is underestimated, the age uncertainty will be overestimated. Therefore, realistically assessing the analytical uncertainty is crucial for detecting true geologic scatter and determining age.

The analytical uncertainty depends on the absolute amount of radiogenic isotopes available for measurement. For apatite, a significant limitation is with the absolute amount of Hf in the sample. Many apatite samples with less than 0.6 ng Hf were either analyzed with shorter integration time or by running at low intensity. Because the Hf analysis is often customized for each sample based on the amount of Hf available, the uncertainty on each isochron point therefore should be individually estimated. The external uncertainty of $^{176}Hf/^{177}Hf$ is often estimated on the basis of its internal measurements statistics as described by Bizzarro *et al.*[23] Multiple analyses of the JMC 475 solution standard measured at different concentrations are used to establish the relationship between internal precision (% 1 s.e.) and external uncertainty (% 2 s.d.) (Table 2 and Fig. 3). The trend is then used to transform the internal precision of samples often measured at lower concentrations than standards into an estimated external uncertainty.

Another source of uncertainty is with interferences on ^{176}Hf from ^{176}Lu to ^{176}Yb. Therefore, it is crucial to eliminate Lu and Yb in the Hf fraction to keep the interference corrections needed at a minimum. The isobaric interferences of ^{176}Lu and ^{176}Yb on ^{176}Hf are monitored by measuring the ^{175}Lu and ^{173}Yb signals during Hf MC-ICPMS analysis (Table 3). The blank Lu is not significant for most Hf-rich whole rocks and moderately high Lu/Hf minerals like garnet because it is usually a few picograms and is often diluted to negligible level in the analyzed Hf solution. However, for the Hf-poor mineral apatite with extremely high Lu/Hf ratio, the blank Lu may account for a portion to all the interfering Lu. The Lu interferences were reported as $^{176}Lu/^{177}Hf$ ratios ranging from 5 ppm to 155 ppm for 18 DGA-normal purified Hf analyses (Table 3). The median ratio reported ($^{176}Lu/^{177}Hf = 0.000091$) corresponds to 0.9 pg of Lu in the analyzed Hf solution, which is lower than the typical lab blank of ~3 pg Lu. This means that blank Lu can cause the measured $^{176}Lu/^{177}Hf$ ratio in the low-Hf solution to be close to 0.0003. However, our purified Hf solutions routinely have this ratio below 0.0003, demonstrating the high performance of the chemical separation scheme. $^{176}Lu/^{177}Hf$ ratios close to or higher than 0.0003 indicate Lu interference from sample and blank.

Typically, the interfering ^{176}Lu and ^{176}Yb are corrected using the measured value for Lu and the natural ratio for Yb. The accuracy of the ^{176}Lu correction, however, is somewhat compromised because the contaminating Lu in Hf consists of variable amounts of residual spiked sample Lu and blank Lu, which is the Lu accumulated along the Hf path through the chemistry. This means that the measured $^{176}Lu/^{175}Lu$ of Lu in the Hf fraction may not correspond perfectly to the $^{176}Lu/^{175}Lu$ of the blank. The isotopic composition of the spiked sample Lu is represented by the measured $^{175}Lu/^{176}Lu$ in the Lu isotope dilution measurement. The blank Lu is generally assumed to have a natural composition ($^{176}Lu/^{175}Lu = 0.02656$). Fortunately, for apatite, correcting using either value leads to no difference in the ages. This is because the Lu is under spiked, as mixed Lu–Hf spike is applied, and the measured Lu ratio (~0.035) is usually not very different from the natural ratio.

Table 2 Internal analysis statistics (% 1 s.e.) and the external reproducibility of replicate analyses (% 2 s.d.) of replicate analyses of the JMC 475 standards at different concentrations

	Mean	1 s.e	2 s.d	*n*
2 ppb	0.282143	0.0030%	0.0118%	14
5 ppb	0.282145	0.0014%	0.0047%	8
10 ppb	0.282142	0.0013%	0.0042%	11
25 ppb	0.282146	0.0010%	0.0036%	30

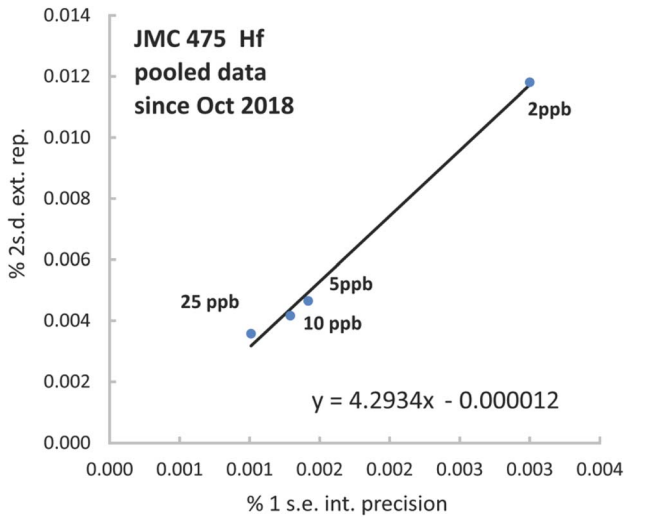

Fig. 3 The relationship between the average internal analysis statistics (% 1 s.e.) and the external reproducibility of replicate analyses (% 2 s.d. of multiple analyses) of the JMC 475 Hf standard analyzed at different concentrations, following the method of Bizzarro *et al.*[23]

Sample testimony

To demonstrate the applicability of the method, we have determined Lu–Hf ages for apatite from three well-known deposits-Otter Lake (Yates Mine), Bancroft, and Durango. The apatite in all occurrences are megacrysts, typically prisms several centimeters long and at least one centimeter in diameter. A summary of age constraints is presented in Table 4.

Otter Lake. The Otter Lake area, Québec, is located north of the Bancroft domain within the Grenville Province and represents the petrography of the Bancroft domain. The studied apatite comes from the Yates Mine locality in the Otter Lake region, where apatite specimens typically take the form of reddish to green, elongated hexagonal prisms with pyramidal terminations set in a hydrothermally altered, salmon-pink calcite and purple fluorite matrix. Barfod *et al.*[13] have dated three apatite fractions from a single crystal and titanite, both from the Otter Lake area, that yielded a Lu–Hf age of 1030.5 ± 5.8 Ma (MSWD = 1.7). The $^{207}Pb/^{206}Pb$ stepwise leaching (PbSL) analyses from five HBr leaching steps, and a bulk dissolution on an aliquot from the same crystal, lie on an isochron of 913 ± 7 Ma (MSWD = 0.24) in $^{207}Pb/^{204}Pb$–$^{206}Pb/^{204}Pb$ space.[46] The titanite analyzed by Barfod *et al.*[13] was previously dated by Frei *et al.*[47] and yields a Pb step-leaching age of 997 ± 10 Ma and a U–

Table 3 Lu, Yb and W interferences observed during Hf isotope analyses with different chemical separation methods. All interferences were monitored as ratios of the stable isotopes over ^{177}Hf isotope, *i.e.*, ^{173}Yb/^{177}Hf, ^{175}Lu/^{177}Hf, ^{182}W/^{177}Hf

		Single-pass Ln column	Ln column plus DGA-normal purification
Number of analyses		23	18
Yb interference (^{176}Yb/^{177}Hf)	Median	0.039238	0.000365
	Min	0.001284	0.000021
	Max	1.095002	0.002505
Lu interference (^{176}Lu/^{177}Hf)	Median	0.002692	0.000091
	Min	0.000197	0.000005
	Max	0.068423	0.000155
W interference (^{182}W/^{177}Hf)	Median	8.16072	0.677053
	Min	1.32641	0.033817
	Max	348.059	3.906926

Table 4 Summary of apatite age constraints from literature

Apatite	Age ± 2σ (Ma)	Method	Ref.
Otter Lake (Yates Mine)			
	1030.5 ± 5.8 Ma	Lu–Hf isochron of three apatite and one titanite	Barfod *et al.* 2003 (ref. 13)
	1042 ± 16 Ma	Lu–Hf isochron of three apatite	Barfod *et al.* 2003 (ref. 13)
	913 ± 7 Ma	PbSL apatite	Barfod *et al.* 2005 (ref. 46)
	997 ± 10 Ma	PbSL titanite	Frei *et al.* 1997 (ref. 47)
	1002 ± 7 Ma	U–Pb titanite	Frei *et al.* 1997 (ref. 47)
	933 ± 12 Ma	U–Pb apatite	Chew *et al.* 2011 (ref. 48)
Bancroft			
	961 ± 13 Ma	U–Pb apatite	Thomson *et al.* 2012 (ref. 16)
	937 ± 20 Ma	U–Pb apatite	Thomson *et al.* 2012 (ref. 16)
	1045–1074 Ma	U–Pb titanite in pegmatite	Mezger *et al.* 1993 (ref. 49)
Durango			
	31.44 ± 0.18 Ma	^{40}Ar/^{39}Ar, weighted mean of four single crystal sanidine-anorthoclase analyses	McDowell *et al.* 2005 (ref. 51)
	31.02 ± 1.01 Ma (1σ)	(U–Th–Sm)/He, weighted mean of 24 apatite analyses	McDowell *et al.* 2005 (ref. 51)

Pb age of 1002 ± 7 Ma. The apatite was also dated using U–Pb by Chew *et al.*[48] and yields a lower-intercept age of 933 ± 12 Ma.

Bancroft. The Bancroft apatite consists of centimeter-sized crystals derived from a pegmatite outcrop in the Bancroft domain of the Grenville Province. The Bancroft domain is dominated by marbles, skarns, amphibolites, and gneisses that underwent greenschist to upper-amphibolite facies metamorphism at temperatures and pressures of 650–700 °C and 6.5–7 kbar in connection with the Elzevirian and Ottowan phases of the Grenville orogeny.[50,51] Additional activity includes a late-stage extension at *ca.* 1045 to 893 Ma within the Bancroft shear zone that separates the Bancroft from the adjacent Elzevir domain. Sphene from skarns, syenite dykes, and widely spread pegmatites within the Bancroft domain yield U–Pb ages that range from 1045 to 1074 Ma (ref. 50) which are significantly older than the U–Pb ages obtained from sphene of unambiguously metamorphic origin (marbles, calc–silicate gneisses), which are in the range of 1045–1030 Ma.[50] One sphene from marble in the north-eastern part of the area gives an age of 1152 Ma for the core and 1141 Ma for the rim.[50] Another sphene from a syenite dyke yields a similarly old age of 1125 Ma suggesting that the regional and contact metamorphism occurred in the intervals of *ca.* 1150 Ma and 1045–1030 Ma in the Bancroft domain.[50] Two Bancroft terrane apatite, one from the Bear Lake region and one from the Wilberforce region, yield apatite U–Pb ages of 961 ± 13 Ma and 937 ± 20 Ma, respectively.[16]

Durango. The Durango apatite is a distinctive lemon-yellow fluorapatite that occurs as exceptional coarse crystals within the open pit iron mine at Cerro de Mercado, on the northern outskirts of Durango City, Mexico. It is a widely distributed reference material for apatite electron microprobe analyses, apatite fission-track, and (U–Th)/He dating/thermochronology. Apatite and iron ore formed *in situ* with emplacement of small felsic intrusions along the southern margin of the Chupaderos caldera complex, which occurred between the eruptions of two major ignimbrites, the Aguila and Santuario ignimbrites, from the caldera. McDowell *et al.*[51] have reported four single-crystal sanidine–anorthoclase ^{40}Ar–^{39}Ar ages from the overlying Santuario formation and underlying Aguila formation and Registro tuff and have bracketed the period of

the Durango apatite at 31.44 ± 0.18 Ma (2σ). The age is in agreement with a set of 24 (U–Th–Sm)/He ages determined directly on the apatite, which have a weighted mean of 31.02 ± 1.01 Ma (1σ).[50]

Results

The Lu–Hf concentrations, isotopic compositions for the analyzed apatite samples are presented in Table 5 and shown in isochron plots in Fig. 4. The external uncertainties applied to measured $^{176}Hf/^{177}Hf$ ratios are individually estimated and is 0.5% for $^{176}Lu/^{177}Hf$, as encountered during the long-term reproducibility of external rock standards. Isochron ages are calculated using the decay constant $\lambda^{176Lu} = 1.867 \times 10^{-11}$ per year.[17,19]

The Otter Lake apatite yield a single mineral isochron age of 1047.6 ± 3.4 Ma (MSWD = 0.47; Fig. 4A). The concentration marbles, skarns, amphibolites, and gneisses that underwent of Hf ranges from 0.014 to 0.110 ppm and is ~6.8 ppm for Lu. The variation on Hf concentration results in extraordinarily high $^{176}Lu/^{177}Hf$ ratios from 8 to 95 and $^{176}Hf/^{177}Hf$ ratios 0.46 to over 2.16 (Table 5). These apatite samples were processed at the last stage of experimenting using most optimized method therefore has little Lu, Yb, W interferences. The variation in the Lu/Hf ratio indicates a heterogeneity on millimeter scale. The age overlaps within uncertainty of the published age (1042 ± 16 Ma)[13] and has smaller age error.

The Bancroft apatite have concentrations ranging from 0.008 to 0.011 ppm for Hf and ~2.8 ppm for Lu resulting in very high $^{176}Lu/^{177}Hf$ ratios from 43 to 130 and $^{176}Hf/^{177}Hf$ ratios from 1.2 to over 1.6. One apatite analysis is displaced above the line defined by three apatite and bulk earth due to the weak Hf signal during MS analysis (Fig. 4B inset). Omitting this analysis from the age calculation results in a Lu–Hf isochron age of 1092 ± 17 Ma (MSWD = 4.7; Fig. 4B). Regression using apatite points only would yield unrealistic initial $^{176}Hf/^{177}Hf$ ratio therefore a calculated initial Hf isotopic composition of CHUR at 1000 Ma was used in the regression and age calculation. The rationale for regression with this model initial value will be discussed below. These samples were analyzed before the DGA-normal clean-up stage was added to the separation procedure and therefore have higher Lu and Yb interferences on Hf which may have compromised the accuracy of some of the apatite analyses.

The Durango apatite have concentrations of 5.3–7.4 ppm for Lu and very low concentration of Hf from 1.6 ppb to 2.4 ppb resulting in extremely high $^{176}Lu/^{177}Hf$ ratios at around 480 resulting in very radiogenic ratio of $^{176}Hf/^{177}Hf = \sim 0.55$. An isochron based on analyses of five apatite fractions and the present-day CHUR $^{176}Hf/^{177}Hf$ of 0.282785 yield an age of 31.1 ± 1.1 Ma (MSWD = 101; Fig. 4C).

Discussion and concluding summary

Apatite Lu–Hf chronometer

The apatite Lu–Hf isochrons are characterized by highly elevated $^{176}Lu/^{177}Hf$ ratios and highly radiogenic $^{176}Hf/^{177}Hf$ ratios due to the low Hf abundance in apatite. These high ratios are advantageous for generating precise ages, especially when jointly applied with a low parent–daughter ratio in age regression. However, this low parent–daughter ratio, usually supplied by the bulk rock or another mineral, can be substituted by an estimated initial $^{176}Hf/^{177}Hf$ ratio without affecting the isochron age. This is because the variance of a reasonable initial $^{176}Hf/^{177}Hf$, compared to the scale of the isochron, is very small and has little effect on changing the slope. As in the case of Bancroft, no whole rock or any other minerals were analyzed and the isochron simply consists of three apatite fractions, all plot on the high end of the isochron. In order to test the effects of different estimated initial $^{176}Hf/^{177}Hf$ ratios on the isochron age, three $^{176}Hf/^{177}Hf$ ratios were calculated, and each plotted with the three apatite fractions to determine an age. The first is the $^{176}Hf/^{177}Hf$ ratio of CHUR at 1000 Ma based on its present-

Table 5 Lu–Hf isotopic data for the apatites

Lu (ppm)	Hf (ppm)	$^{176}Lu/^{177}Hf$	$^{176}Hf/^{177}Hf$	Err	Age ± 2σ
Otter Lake (Yates Mine)					
6.54	0.110	8.677	0.45755	±0.00034	1047.6 ± 3.4
6.84	0.021	55.11	1.37632	±0.00077	MSWD = 0.47
6.70	0.014	92.75	2.11469	±0.00173	
7.16	0.014	95.09	2.16498	±0.00120	
Bancroft					
2.82	0.005	130.5	3.13406	±0.01156	1092 ± 17 Ma
2.89	0.010	46.18	1.22215	±0.01515	MSWD = 4.7
2.88	0.008	64.76	1.61046	±0.00020	
2.87	0.011	43.70	1.18725	±0.00008	
Durango					
5.45	0.0016	517.8	0.57158	±0.00034	31.1 ± 1.1 Ma
5.56	0.0018	458.7	0.55131	±0.00080	MSWD = 101
7.41	0.0024	468.2	0.56196	±0.00042	
6.55	0.0020	480.6	0.56410	±0.00014	
5.32	0.0017	483.2	0.55616	±0.00172	

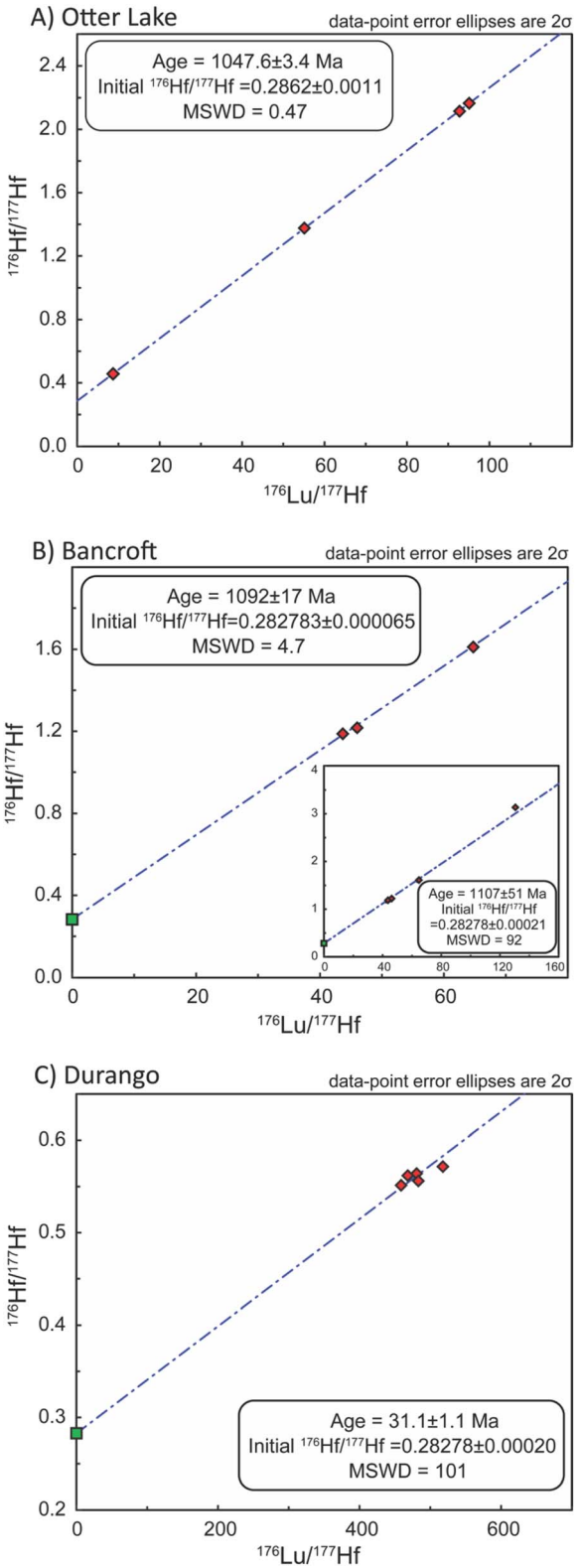

Fig. 4 Lu–Hf isochron plots for (A) Otter Lake, (B) Bancroft, (C) Durango. Apatite points are red and are shown either as error ellipses or diamonds when errors are too small. Green square points represent bulk earth.

day $^{176}Hf/^{177}Hf$ and $^{176}Lu/^{177}Hf$ values of 0.282785 and 0.0336, respectively.[52] The second is the $^{176}Hf/^{177}Hf$ ratio of an enriched crust reservoir at 1000 Ma with a $^{176}Lu/^{177}Hf$ value of 0.015.[53] The third is the depleted mantle $^{176}Hf/^{177}Hf$ ratio at 1000 Ma using present-day $^{176}Hf/^{177}Hf$ and $^{176}Lu/^{177}Hf$ values of 0.283225 and 0.038512, respectively.[45] These three values are calculated to be 0.282151, 0.281135, and 0.282505 and represent the range of all the reasonable initial $^{176}Hf/^{177}Hf$ ratios in different terrestrial reservoirs. The regressions of each of the values with three apatite fractions yield isochrons and ages shown in Fig. 5. Two of the three ages are the same with the third being only 1 Ma (<0.1%) older. This demonstrates that because the scale of the isochron, leveraged by the high $^{176}Hf/^{177}Hf$ ratio of apatite, is much larger than the variance of $^{176}Hf/^{177}Hf$ ratio among all the terrestrial reservoirs at the approximate age of the sample; such small variance on one end of the regression line makes an insignificant change on the slope and thus has little effect on the isochron age. Thus, the apatite Lu–Hf isochron essentially can be anchored with the isotope composition of CHUR at the approximate age of the sample without compromising the accuracy and precision of the age. Following this reasoning, the age regression of Durango was calculated based on the apatite fractions and the present-day CHUR isotope composition. This does mean that apatite Lu–Hf has a constitutional deficiency in defining the initial ratio because the data points are far from the longitudinal axis.

Comparison to the laser-ablation method

Recently, some studies have employed the laser-ablation based method to obtain *in situ* Lu–Hf ages for apatite samples (*e.g.*, Simpson *et al.*,[54] Wu *et al.*[55]). This method offers benefits such as optimized spatial resolution, rapid analysis, and high data production rate that enable detritus provenance studies. However, it can pose challenges in determining the ^{176}Lu and ^{176}Yb isobaric interferences on the ^{176}Hf signal (*e.g.*, Woods[56]), a critical factor for precise Lu–Hf age determination, particularly in cases of samples with low Hf content and young age (*e.g.*, Durango apatite). Our approach takes advantage of the effective removal of interfering elements such as Lu, Yb, and W, and the successful recovery of nearly 100% of Hf from three well-characterized apatite reference materials. Additionally, a main issue of laser ablation analyses is lower precision

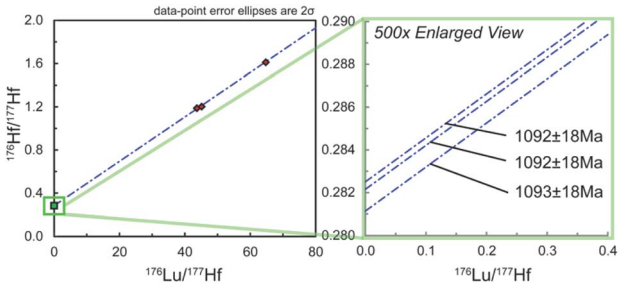

Fig. 5 Lu–Hf isochron plots for Bancroft apatite using three apatite points (red diamond) and three different initial values-$^{176}Hf/^{177}Hf$ of CHUR, depleted mantle and enriched crust calculated at 1000 Ma-yield three very similar ages. Variance among the three estimated initial $^{176}Hf/^{177}Hf$ ratios on the longitudinal axis was enlarged 500 times and shown on the right.

compared to solution-based methods. For instance, in the case of Otter Lake apatite, the uncertainty associated with our 4-points Lu–Hf isochron age (1047.6 ± 3.4 Ma, Fig. 4A) amounts to 0.3%. While the uncertainty on the weighted mean Lu–Hf age of 40 analytical spots (1053 ± 12 Ma, Simpson *et al.*[54]) stands at 1.1%, demonstrating that the *in situ* method reduces precision. It is worth noting that the *in situ* Lu–Hf age is older than the solution Lu–Hf age reported by Barfod *et al.*[13] (1030.5 ± 5.8 Ma) and this study.

Applications and limitations of the method

All apatite Lu–Hf ages are in excellent agreement with published ages using different radioactive dating systems, which proves the validity of the Lu–Hf apatite method. The method proves to be working even at very challenging conditions (*e.g.*, sub-nano gram Hf extraction and analysis). The apatite Lu–Hf isochron method has potential in dating a wide range of rocks as apatite group minerals are common accessory minerals found in almost all igneous, metamorphic, and sedimentary rocks. Especially in some mafic rocks that are lacking conventional dateable mineral phases (*e.g.*, zircon, monazite), apatite as a minor phase might be the only datable mineral that provides meaningful geochronologic information. The ability to date apatite offers a number of exciting prospects for constraining ages of the mineralization and metasomatic alteration occurring in a range of apatite deposits. This method will find application in dating these types of magnetite-apatite deposits as sufficient apatite is present. More importantly, it directly dates the magnetite-apatite mineralization compared to other methods that only provide relative age information by dating phases in host rocks. The low Hf content in apatite, and relatively big sample size required in this method, however, may challenge the applicability to igneous and metamorphic rock where apatite is a minor phase.

Conflicts of interest

There are no conflicts to declare.

Acknowledgements

We thank Victor A. Valencia and Christopher M. Fisher for providing valuable research samples. We gratefully acknowledge Da Wang's assistance in facilitating the mass spectrometry analyses. Thanks also go to two anonymous reviewers for their thorough reviews and constructive comments.

References

1 R. H. Jones, F. M. McCubbin, L. Dreeland, Y. Guan, P. Burger and C. K. Shearer, *Geochim. Cosmochim. Acta*, 2014, **132**, 120–140.
2 J. W. Boyce, Y. Liu, G. R. Rossman, Y. Guan, J. M. Eiler, E. M. Stolper and L. A. Taylor, *Nature*, 2010, **466**, 466–469.
3 J. F. Rakovan and J. D. Pasteris, *Elements*, 2015, **11**, 195–200.
4 Y. Pan and M. E. Fleet, *Rev. Mineral. Geochem.*, 2002, **48**, 13–49.
5 A. L. Doherty, J. D. Webster, B. A. Goldoff and P. M. Piccoli, *Chem. Geol.*, 2014, **384**, 94–111.
6 E. C. Hansen and D. E. Harlov, *J. Petrol.*, 2007, **48**, 1641–1680.
7 R. Sallet, *Lithos*, 2000, **50**, 241–253.
8 D. E. Harlov, U. B. Andersson, H.-J. Förster, J. O. Nyström, P. Dulski and C. Broman, *Chem. Geol.*, 2002, **191**, 47–72.
9 J. Krause, D. E. Harlov, E. V. Pushkarev and G. E. Brügmann, *Geochim. Cosmochim. Acta*, 2013, **121**, 503–521.
10 G. Palma, F. Barra, M. Reich, V. Valencia, A. C. Simon, J. Vervoort, M. Leisen and R. Romero, *Geochim. Cosmochim. Acta*, 2019, **246**, 515–540.
11 D. M. Chew and R. A. Spikings, *Elements*, 2015, **11**, 189–194.
12 D. M. Chew and R. A. Donelick, *EGU General Assembly Conference Abstracts*, 2012, p. 1192.
13 G. H. Barfod, O. Otero and F. Albarède, *Chem. Geol.*, 2003, **200**, 241–253.
14 C. L. Kirkland, C. Yakymchuk, K. Szilas, N. Evans, J. Hollis, B. McDonald and N. J. Gardiner, *Lithos*, 2018, **318–319**, 143–157.
15 D. Larsson and U. Söderlund, *Chem. Geol.*, 2005, **224**, 201–211.
16 S. N. Thomson, G. E. Gehrels, J. Ruiz and R. Buchwaldt, *Geochem., Geophys., Geosyst.*, 2012, **13**, Q0AA21.
17 E. Scherer, C. Munker and K. Mezger, *Science*, 2001, **293**, 683–687.
18 E. Scherer, K. Mezger and C. Munker, *AGU Fall Meeting Abstracts*, 2002, V52B-1293.
19 U. Söderlund, P. J. Patchett, J. D. Vervoort and C. E. Isachsen, *Earth Planet. Sci. Lett.*, 2004, **219**, 311–324.
20 V. Debaille, J. Van Orman, Q.-Z. Yin and Y. Amelin, *Earth Planet. Sci. Lett.*, 2017, **473**, 52–61.
21 F. K. Crundwell, *Hydrometallurgy*, 2016, **161**, 34–44.
22 P. J. Patchett and M. Tatsumoto, *Contrib. Mineral. Petrol.*, 1981, **75**, 263–267.
23 M. Bizzarro, J. A. Baker and D. Ulfbeck, *Geostand. Newsl.*, 2003, **27**, 133–145.
24 D. Ulfbeck, J. Baker, T. Waight and E. Krogstad, *Talanta*, 2003, **59**, 365–373.
25 B. Le Fèvre and C. Pin, *Anal. Chem.*, 2001, **73**, 2453–2460.
26 J. Blichert-Toft, C. Chauvel and F. Albarède, *Contrib. Mineral. Petrol.*, 1997, **127**, 248–260.
27 R. Anczkiewicz, J. P. Platt, M. F. Thirlwall and J. Wakabayashi, *Earth Planet. Sci. Lett.*, 2004, **225**, 147–161.
28 A. F. Bird, M. F. Thirlwall, R. A. Strachan and C. J. Manning, *J. Geol. Soc.*, 2013, **170**, 301–317.
29 H. Cheng, R. L. King, E. Nakamura, J. D. Vervoort and Z. Zhou, *J. Metamorph. Geol.*, 2008, **26**, 741–758.
30 S. R. Mulcahy, R. L. King and J. D. Vervoort, *Geology*, 2009, **37**, 987–990.
31 M. A. Smit, E. E. Scherer and K. Mezger, *Earth Planet. Sci. Lett.*, 2013, **381**, 222–233.
32 R. Bast, E. E. Scherer, P. Sprung, M. Fischer-Gödde, A. Stracke and K. Mezger, *J. Anal. At. Spectrom.*, 2015, **30**, 2323–2333.

33 E. P. Horwitz, M. L. Dietz, R. Chiarizia, H. Diamond, A. M. Essling and D. Graczyk, *Anal. Chim. Acta*, 1992, **266**, 25–37.
34 C. Münker, S. Weyer, E. Scherer and K. Mezger, *Geochem., Geophys., Geosyst.*, 2001, **2**, 1064.
35 G. Goldstein, *Anal. Chem.*, 1964, **36**, 243–244.
36 J. R. Van Wazer and C. F. Callis, *Chem. Rev.*, 1958, **58**, 1011–1046.
37 T. R. Dulski, *A Manual for the Chemical Analysis of Metals*, 1996, vol. 75.
38 J. N. Connelly, D. G. Ulfbeck, K. Thrane, M. Bizzarro and T. Housh, *Chem. Geol.*, 2006, **233**, 126–136.
39 Y. Amelin, *Science*, 2005, **310**, 839–841.
40 C. Pin and J. S. Zalduegui, *Anal. Chim. Acta*, 1997, **339**, 79–89.
41 E. P. Horwitz and C. A. A. Bloomquist, *J. Inorg. Nucl. Chem.*, 1975, **37**, 425–434.
42 J. D. Vervoort, P. J. Patchett, U. Söderlund and M. Baker, *Geochem., Geophys., Geosyst.*, 2004, **5**, Q11002.
43 E. P. Horwitz, D. R. McAlister, A. H. Bond and R. E. Barrans, *Solvent Extr. Ion Exch.*, 2005, **23**, 319–344.
44 A. Pourmand and N. Dauphas, *Talanta*, 2010, **81**, 741–753.
45 J. D. Vervoort and J. Blichert-Toft, *Geochim. Cosmochim. Acta*, 1999, **63**, 533–556.
46 G. H. Barfod, E. J. Krogstad, R. Frei and F. Albarède, *Geochim. Cosmochim. Acta*, 2005, **69**, 1847–1859.
47 R. Frei, I. M. Villa, Th. F. Nägler, J. D. Kramers, W. J. Przybylowicz, V. M. Prozesky, B. A. Hofmann and B. S. Kamber, *Geochim. Cosmochim. Acta*, 1997, **61**, 393–414.
48 D. M. Chew, P. J. Sylvester and M. N. Tubrett, *Chem. Geol.*, 2011, **280**, 200–216.
49 K. Mezger, E. J. Essene, B. A. van der Pluijm and A. N. Halliday, *Contrib. Mineral. Petrol.*, 1993, **114**, 13–26.
50 R. Kretz, J. L. Campbell, E. L. Hoffman, R. Hartree and W. J. Teesdale, *J. Metamorph. Geol.*, 1999, **17**, 41–59.
51 F. W. McDowell, W. C. McIntosh and K. A. Farley, *Chem. Geol.*, 2005, **214**, 249–263.
52 A. Bouvier, J. D. Vervoort and P. J. Patchett, *Earth Planet. Sci. Lett.*, 2008, **273**, 48–57.
53 J. W. Goodge and J. D. Vervoort, *Earth Planet. Sci. Lett.*, 2006, **243**, 711–731.
54 A. Simpson, S. Gilbert, R. Tamblyn, M. Hand, C. Spandler, J. Gillespie, A. Nixon and S. Glorie, *Chem. Geol.*, 2021, **577**, 120299.
55 S. Wu, H. Wang, Y. Yang, J. Niu, Z. Lan, L. Zhang, C. Huang, L. Xie, L. Xu, J. Yang and F. Wu, *J. Anal. At. Spectrom.*, 2023, **38**, 1285–1300.
56 G. Woods, *Agilent Application Note*, 2016, 5991-6787EN.